JCTC Journal of Chemical Theory and Computation

Article

pubs.acs.org/JCTC

Gluing Potential Energy Surfaces with Rare Event Simulations

Anders Lervik and Titus S. van Erp*

Department of Chemistry, Norwegian University of Science and Technology, 7491 Trondheim, Norway

ABSTRACT: We develop a new method combining replica exchange transition interface sampling with two distinct potential energy surfaces. The method can be used to combine different levels of theory in a simulation of a molecular process (e.g., a chemical reaction), and it can serve as a dynamical version of QM-MM, connecting classical dynamics with Ab Initio dynamics in the time domain. This new method, which we coin QuanTIS, could be applied to use accurate but expensive density functional theory based molecular dynamics for the breaking and making of chemical bonds, while the diffusion of reactants in the solvent are treated with classical force fields. We exemplify the method by applying it to two simple model systems (an ion dissociation reaction and a classical hydrogen model), and we discuss a possible extension of the method in which classical force field parameters for chemical reactions can be optimized on the fly.

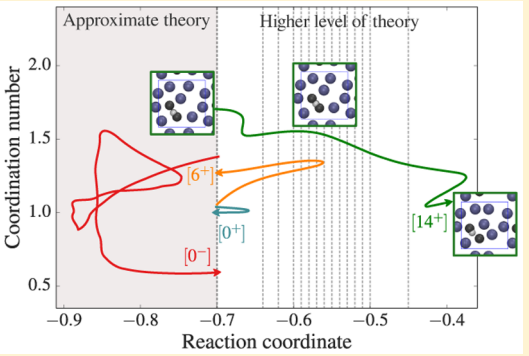

1. INTRODUCTION

Many processes in nature arise from the spontaneous transition between stable states separated by an activation barrier. If the activation barrier is sufficiently high, a transition between the stable states can be considered a rare event as the probability of a fluctuation driving the transition decreases exponentially with the activation barrier. The time scale for the overall transition (e.g., milliseconds) can be many orders of magnitude larger than the molecular time scale (e.g., femtoseconds), and this poses a challenge for simulation techniques which aim to accurately model rare events.

In principle, molecular dynamics (MD) could be used as a computational tool to investigate such transitions, but for rare events this is not feasible: The time scale required to accurately simulate the transition is far greater than what is currently attainable by MD simulations. A brute-force MD simulation becomes inefficient as the trajectory mainly samples the stable states, and only a tiny fraction of it corresponds to the transition itself. Further, in order to correctly model the reactive event, an accurate description of the energy landscape is needed. For this purpose, one could make use of a reactive force field; but this is often not accurate enough, and calculations using a more detailed description, e.g. on the quantum mechanical (QM) level, are required. This would significantly increase the cost of a MD-based approach, and we are thus faced with two interconnected challenges: reaching the relevant time scale while maintaining an acceptable accuracy.

In order to tackle these challenges, several methods have been proposed over the last decades. Hyperdynamics[1] aims at lowering the energy difference between the top of the barrier and the initial basin, the parallel replica method[2] exploits the power of parallel processing to extend the molecular simulation time, and temperature-accelerated dynamics[3] speeds up the event by raising the temperature. The idea of driving energy into the system to escape the basin of the energy minimum in which the system is initially prepared is also at the basis of conformational flooding[4] and the metadynamics method.[5] Other important methods are thermodynamic integration[6] and umbrella sampling,[7] eigenvector following,[8] the activation-relaxation technique,[9] nudged elastic band,[10] string method,[11] and discrete path sampling.[12] These methods have in common that they enhance reactive events by perturbing the actual dynamics. Using reweighting schemes, based on the laws of statistical physics, one can usually get exact results on (static) statistics such as free energy barriers, but important information on the spontaneous dynamical process is usually lost. Moreover, free energies expressed as a low dimensional function of a set of reaction coordinates can be very misleading. The height of free energy barriers depend sensitively on the set of reaction coordinates that is chosen. As a result, Transition State Theory (TST) is insufficient to make predictions about reaction rates in complex systems. The reactive flux method[13] is the standard approach to correct the TST expression. It complements the free energy calculation along a single reaction coordinate with the calculation of a dynamical transmission coefficient, by starting short trajectories from the maximum of the free energy barrier. However, in complex systems the correct reaction coordinate can be exceedingly difficult to find. If the reaction coordinate does not capture the molecular mechanism, the biased sampling methods will suffer from substantial hysteresis when following the system over the barrier. Moreover, even if the free energy profile is obtained correctly for this particular (but wrong) reaction coordinate, the corresponding transmission coefficient will be very low, making an accurate evaluation problematic.

Received: January 7, 2015
Published: April 24, 2015

DOI: 10.1021/acs.jctc.5b00012
J. Chem. Theory Comput. 2015, 11, 2440−2450

In order to overcome these difficulties, Chandler and coworkers[14−16] developed the transition path sampling (TPS)[17,18] method which does not require detailed knowledge of the transition state (or the reaction coordinate/mechanism). In fact, the transition state and the reaction mechanism can be inferred from the results of a TPS simulation. The TPS method uses a Monte Carlo (MC) approach to sample reactive trajectories connecting an initial and final state. This is combined with the probability of reaching the final state from the initial state (obtained by an umbrella sampling approach) in order to estimate the rate constant for the transition. Transition interface sampling (TIS)[19] builds on the TPS approach and improves the efficiency by allowing flexible path lengths, it is less sensitive to recrossings, and the umbrella sampling technique is replaced by interface ensemble averages.[19] In addition, the MC technique in the TIS method is simpler since it only involves the so-called *shooting* move and not both *shooting* and *shifting* moves as in the TPS method. The TIS method has been further developed into the replica exchange TIS (RETIS)[20] approach, where replica exchange moves are carried out between the different path simulations. This represents a significant improvement in efficiency compared with the standard TIS method. The RETIS method is also better suited to tackle complex reaction mechanisms with many degrees of freedom and multiple reaction channels.[21,22] For completeness, we also mention the recent combined methods in which TPS/TIS is combined with thermodynamic integration type of approaches[23−25] or metadynamics.[26]

Both the TIS and the RETIS methods introduce a set of interfaces between the reactant and the product state and recasts the overall crossing probability as a product of crossing probabilities for the intermediate interfaces. In order to estimate the rate constant for the transition, the TIS method combines this probability with a MD-simulation where the escape flux through the first interface is calculated. In the RETIS approach, the escape flux is calculated using the average path lengths in the two ensembles associated with the first interface. These two ensembles can be interpreted as corresponding to different processes: nonreactive exploration of the stable reactant state and the initial progress of the reactive event. It is this interpretation that forms the basis of the new method we introduce in this article.

Even though the path-ensemble methods can be many times more efficient than a MD-based approach, they are still dependent on an accurate description of the energy landscape. This will often require expensive calculations (e.g., on the QM level). One way to reduce the cost is to limit the QM treatment to certain spatial regions of the system and treat the rest with a classical method. Such quantum mechanics-molecular mechanics (QM-MM)[27,28] methods have successfully been used together with TPS[29−32] to boost the accuracy and attainable length scale of the system under consideration. This requires that one can, a priori, select which regions require a QM or MM treatment. In this context, the interpretation of the two ensembles associated with the first interface in the RETIS approach points to an alternative strategy for decreasing the computational cost: The ensemble corresponding to nonreactive exploration can be treated with a less detailed theory (e.g., MM) than the other ensembles (e.g., QM). Effectively, this corresponds to a dynamical QM-MM approach, where different accuracies are used in different path ensembles and the choice of employing QM or MM is based on the temporal rather than the spatial coordinate. In this new approach, which we coin QuanTIS, the system is *either* treated fully with QM or fully with MM at a given time. This is advantageous since the path lengths corresponding to the nonreactive exploration can be made considerably longer than the path lengths in the other ensembles by positioning the first interface at the barrier region. A significant reduction in the computational cost can be attained by applying the more (computationally) expensive theory only to the reaction itself.

The aim of this article is to introduce this new QuanTIS method, exemplify it, and discuss the prospects of the approach. We begin by discussing the RETIS approach in more detail since this is the theoretical basis of the QuanTIS method. As a proof of concept, we investigate two different systems: (I) a model of a hypothetical ion transfer system where a solvent may reduce the transfer barrier and (II) a realistic model for the dissociation of hydrogen molecules. These models are defined before we discuss the computational details in section 4 and our results in section 5. We provide a perspective on the outlook for the new QuanTIS approach, and we propose further applications before we end with the final conclusion.

2. THEORY

The RETIS method is a very efficient strategy for performing path simulations. In this section, we give a brief summary of the approach, before we discuss the new strategy of applying different levels of theory for the path ensembles connected to the first interface. We then discuss the two systems we consider for testing the QuanTIS method.

2.1. Replica Exchange Transition Interface Sampling.

For the discussion of the RETIS approach, we consider a transition between two stable states, labeled A (the reactant) and B (the product), and we assume that the transition is a rare event. In the RETIS approach we first select a reaction coordinate, $\lambda(R^N, p^N)$, which in general depends on the positions (R^N) and momenta (p^N) of all the N particles, and we define a set of interfaces $\lambda_0, \lambda_1, ..., \lambda_n$, such that the first interface is the boundary of state A (i.e., the system is in state A for $\lambda \leq \lambda_0 = \lambda_A$) and the last interface is the boundary of the product (i.e., the system is in state B for $\lambda \geq \lambda_n = \lambda_B$). The other interfaces are positioned to maximize the efficiency of the method and the rate constant for the transition from A to B, k_{AB}, can be obtained by

$$k_{AB} = f_A \mathcal{P}_A(\lambda_B|\lambda_A) \tag{1}$$

where f_A is the flux through the first interface and $\mathcal{P}_A(\lambda_B|\lambda_A)$ is the probability of crossing λ_B before λ_A given that λ_A was crossed in the past. In practice, it is more convenient to estimate the rate constant by expanding the probability as

$$k_{AB} = f_A \mathcal{P}_A(\lambda_B|\lambda_A) = f_A \prod_{i=0}^{n-1} \mathcal{P}_A(\lambda_{i+1}|\lambda_i) \tag{2}$$

where $\mathcal{P}_A(\lambda_{i+1}|\lambda_i)$ is the probability of a path crossing λ_{i+1} given that it originated in λ_A, ended in λ_A or λ_B, and had at least one crossing with λ_i. In order to calculate these probabilities, we define $[i^+]$ as the collection of paths that start at λ_A and has at least one crossing with λ_i before revisiting λ_A or ending at λ_B. The probability $\mathcal{P}_A(\lambda_{i+1}|\lambda_i)$ can then be obtained as the fraction of paths in the $[i^+]$ ensemble that cross λ_{i+1} as well.

The approach discussed so far corresponds to the conventional TIS method,[19] and f_A is then obtained by performing a MD simulation. For the RETIS approach, replica exchange moves, or swapping moves, are attempted between paths corresponding to different path ensembles. In order to have full flexibility in the swapping moves the MD simulation in the TIS method is

DOI: 10.1021/acs.jctc.5b00012
J. Chem. Theory Comput. 2015, 11, 2440−2450

replaced by another path ensemble $[0^-]$ which corresponds to all paths that start at λ_A, then go in the negative direction, and end back at λ_A. Defining $\langle t_{\text{path}}^{[k]} \rangle$ as the average path length in the $[k]$ path ensemble, the flux through the first interface is then obtained from

$$f_A = \left(\langle t_{\text{path}}^{[0^-]} \rangle + \langle t_{\text{path}}^{[0^+]} \rangle \right)^{-1} \tag{3}$$

The algorithm for the RETIS method is as follows:[20] At each step it is (with equal probability) decided whether to perform *shooting* or *swapping* moves. In the first case, all the path simulations are updated sequentially with a shooting move. In the latter case, swaps will be attempted between the different path simulations, and it is again decided with equal probability if swaps between the ensembles $[0^-] \leftrightarrow [0^+]$, $[1^+] \leftrightarrow [2^+]$, etc. or between the ensembles $[0^+] \leftrightarrow [1^+]$, $[2^+] \leftrightarrow [3^+]$, etc. are attempted. If the swapped paths are not valid, the move is rejected, and the old paths are recounted in the two ensembles involved in the swap. For the swapping between ensembles $[0^-]$ and $[0^+]$ new trajectories are generated in the following way: The last step of the old path in $[0^-]$ is used as the initial point for generating a new trajectory for $[0^+]$ by integrating forward in time, while the initial point in the old path in $[0^+]$ is used to generate a new path for $[0^-]$ by integrating backward in time.

The description so far corresponds to the case where we treat all path ensembles with the same level of theory. In the new QuanTIS approach, we will use an approximate theory in the $[0^-]$ ensemble and a higher level of theory in $[0^+]$ and all other ensembles. In order to ensure detailed balance in the MC sampling within the two levels of theories the following acceptance rule must be fulfilled before the swap $[0^-] \leftrightarrow [0^+]$ is accepted

$$P_{\text{acc}}(r_{\text{lo}}, r_{\text{hi}}) = \text{MIN}\left[1, \exp\left(-\frac{1}{k_B T}[V_{\text{hi}}(r_{\text{lo}}) - V_{\text{lo}}(r_{\text{lo}}) + V_{\text{lo}}(r_{\text{hi}}) - V_{\text{hi}}(r_{\text{hi}})]\right)\right] \tag{4}$$

where V_{hi} and V_{lo} denote the potential energy calculated with the higher level of theory and with the more approximate theory, respectively. We note that a similar expression appears in Li and Yang[33] where it is used to enhance configurational sampling in QM space using a MM force field.

These energies are evaluated at the λ_A interface using r_{lo}, the last point from the path in $[0^-]$, and r_{hi}, the initial point from the path in $[0^+]$. Another technicality is that, in the QuanTIS method, one needs to ensure that the interface is still crossed in a single time step for the phase points that are being swapped. In practice, this is done by swapping the very first phase point of the $[0^+]$ ensemble which is at the left side of λ_A and the one but last phase point of the $[0^-]$ ensemble that is also still at the left side of this interface. Then, in addition of the acceptance rule 4 we require that the next forward MD step starting from these points based on the new potentials will both create a point that is at the right side of λ_A. Otherwise, the move is rejected. The acceptance rule ensures that the crossing probability remains exact at the high level description of theory. However, since the acceptance rule 4 depends exponentially on the energy differences between potentials V_{lo} and V_{hi} for configuration points at the first interface, the acceptance can be low and the swapping move becomes inefficient if the two levels of theory are too different. This point is further discussed in section 6.

The flux factor f_A, on the other hand, becomes an average of the low and high level fluxes via eq 3. In practice, the interfaces will be chosen such that $t_{\text{path}}^{[0^-]} \gg t_{\text{path}}^{[0^+]}$ implying that the flux factor in the QuanTIS approach will be mostly resembling the flux of the low level system. This is not necessarily affecting the accuracy of the result in a negative manner. Classical force fields have been fitted extensively to reproduce solvent dynamics and are, therefore, often more accurate for that aspect than Ab Initio MD.[34]

2.2. Models. In order to exemplify our new method and as a proof of concept, we consider two model reactions: (I) A hypothetical ion transfer between two identical particles where solvent particles may reduce the barrier to the transfer (i.e., a cooperative effect); (II) the spontaneous dissociation of hydrogen using force field from literature.[35]

For the first example, the high level of theory corresponds to the full interaction potential, while the approximate theory ignores the cooperative effect. For the second example, a many-body effect is included in the high level of theory (via a three-body interaction) which is neglected in the approximate theory. This three-body term effectively forbids the formation of hydrogen clusters, H_n with $n > 2$, and this behavior is preserved by adding a simple repulsive term to the approximate potential.

We will in the following describe these models in more detail.

2.2.1. Cooperative Ion Potential. The cooperative ion potential models an ion transfer according to Ax + A → A + Ax, where the presence of a solvent (particles of type B) may reduce the barrier for the transfer. All particles, A, B, and x, are treated as two-dimensional point particles with identical mass. In the following, we will assume that we only have one particle of type x and two particles of type A.

The total interaction energy, V_{tot}, is given by

$$V_{\text{tot}}(\mathbf{r}_1, \mathbf{r}_2, ..., \mathbf{r}_n) = \sum_{i=1}^{N-1} \sum_{j=i+1}^{N} V_{ij}(r_{ij}) + V_{\text{coop}}(\mathbf{r}_1, \mathbf{r}_2, ..., \mathbf{r}_n) \tag{5}$$

where V_{ij} describes the pair interaction between atom i and j, $r_{ij} = |\mathbf{r}_i - \mathbf{r}_j|$, and V_{coop} describes the cooperative effect. The pair interaction V_{ij} is based on the Lennard-Jones potential with parameters ϵ_{ij}, σ_{ij}, and cutoff r_{ij}^c. Interactions between particles of type A and x are modeled by a shifted Lennard-Jones potential, while all other interactions are modeled by the Weeks−Chandler−Andersen (WCA) potential with cut-offs given by $r_{ij}^c = 2^{1/6}\sigma_{ij}$ (see eqs 20− 22 in the Appendix). The parameters for the pair interactions are given in Table 1 where we also show the potential energies for the different pairs as a function of the distance in the inset figure.

The cooperative part of the potential is modeled as

$$V_{\text{coop}} = -F(n) \times (V_{\text{cluster}} + \epsilon_{\text{xA}}) \tag{6}$$

where $F(n)$ is a function of the coordination number (n, defined below) for particles of type B around x, and V_{cluster} is the total pair interaction energy of the x and A particles (see eq 23 in the Appendix). Here, ϵ_{xA} is the Lennard-Jones parameter for the x−A pair. The coordination number for solvent particles of type B around x is

$$n = \sum_{j \in \{\text{type B}\}} H(r_{xj}; R_{\text{coop}}, N_d) \tag{7}$$

where R_{coop} and N_d are parameters, and H is a smooth step function defined by

DOI: 10.1021/acs.jctc.5b00012
J. Chem. Theory Comput. 2015, 11, 2440−2450

Table 1. Parameters (in Reduced Units) for the Pair Interactions in the Ion Potential[a]

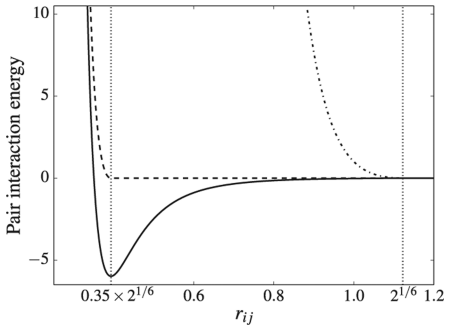

pair (ij)	ϵ_{ij}	σ_{ij}	r_{ij}^c	potential
AB, AA, BB	1	1	$2^{1/6}$	WCA
xA	6	0.35	$2^{1/6}$	Shifted LJ
xB	6	0.35	$0.35 \times 2^{1/6}$	WCA

[a]The interactions are modeled using the Weeks−Chandler−Andersen (WCA) potential or a shifted 6-12 Lennard-Jones potential (Shifted LJ) as described in the text. In the inset figure, the pair interaction potential energies are shown as a function of the particle−particle distance (r_{ij}) in reduced units. The solid line is the x−A pair interaction, the dashed line is the x−B pair interaction, and the dash-dotted line is the A−B, A−A, and B−B pair interactions. The two vertical dotted lines are the cut-offs, $0.35 \times 2^{1/6}$ and $2^{1/6}$, and as the figure shows, only the x−A pair interaction has an attractive part.

$$H(r;\, R,\, M) = \frac{1}{1 + \exp[M(r - R)]} \tag{8}$$

Finally, the function F is the defined as

$$F(n) = f_c \times [1 - H(n;\, N_c,\, N_n)] \tag{9}$$

where $f_c \geq 0$, and N_c and N_n are parameters. The function $H(n; N_c, N_n)$ interpolates smoothly between 0 for large coordination numbers and 1 for small coordination numbers corresponding to $V_{coop} = -f_c \times (V_{cluster} + \epsilon_{xA}) \leq 0$ and $V_{coop} = 0$, respectively. In the ground state, where x is bound to one A and the other A particle is at a distance where it is only interacting with B particles, $V_{cluster} \approx -\epsilon_{xA}$, which also implies that $V_{coop} \approx 0$; the cooperative effect lowers the potential energy of the barrier without effecting the ground state energy (see Figure 4 in the Appendix), effectively reducing the barrier for ion transport. For the cooperative part of the potential, we set $N_d = 20$, $N_n = 20$, and $N_c = 1.1$. The remaining two parameters, R_c and f_c, can be used to tune the strength of the cooperative effect, and we will consider these two parameters in more detail when we describe our test cases in section 3.

2.2.2. Dissociation of Hydrogen. The hydrogen interaction is modeled using the potential described by Kohen et al.,[35] which consists of two- and three-body interactions. For a collection of hydrogen atoms, the potential energy is given by

$$V(\mathbf{r}_1, \mathbf{r}_2, \ldots, \mathbf{r}_n) = \sum_{i>j} V_{ij}(r_{ij}) + \sum_{i>j>k} V_{ijk}(\mathbf{r}_i, \mathbf{r}_j, \mathbf{r}_k) \tag{10}$$

where $\mathbf{r}_i$ is the position of hydrogen atom i, and V_{ij} and V_{ijk} denote the interaction between pairs (ij) and triplets (ijk) of hydrogen atoms, respectively. The two-body term is here completely determined by the relative distance, $r_{ij} = |\mathbf{r}_i - \mathbf{r}_j|$, and it is given by

$$V_{ij}(r_{ij}) = \alpha(\beta r_{ij}^{-4} - 1) \exp[\gamma_2/(r_{ij} - r_c)] \tag{11}$$

when $r_{ij} < r_c$, and it is zero otherwise. The parameters are[35,36] α = 804.959233 kcal/mol, β = 0.044067 Å^4, γ_2 = 3.902767 Å, and r_c = 2.8 Å, and the minimum of the pair interaction for this set of parameters is approximately at a distance 0.74 Å, corresponding to the bond distance of H_2.

The three-body term is given by

$$V_{ijk}(\mathbf{r}_i, \mathbf{r}_j, \mathbf{r}_k) = h(r_{ij}, r_{kj}, \theta_{ijk}) + h(r_{ji}, r_{ki}, \theta_{jik}) + h(r_{ik}, r_{jk}, \theta_{ikj}) \tag{12}$$

where the function $h\,(r_{ij}, r_{kj}, \theta_{ijk}) = h_{ijk}$ is

$$h_{ijk} = \xi(1 + \mu\cos(\theta_{ijk}) + \nu\cos^2(\theta_{ijk})) \times \exp(\gamma_3/(r_{ij} - r_c) + \gamma_3/(r_{kj} - r_c)) \tag{13}$$

if both $r_{ij} < r_c$ and $r_{kj} < r_c$, and zero otherwise. The middle index for each triplet refers to the center atoms for the angle (see also Figure 5 in the Appendix)

$$\cos\theta_{ijk} = \frac{\mathbf{r}_{ij} \cdot \mathbf{r}_{kj}}{r_{ij} r_{kj}} \tag{14}$$

and the parameters are[35,36] ξ = 403.005 kcal/mol, μ = 0.132587, ν = −0.2997, and γ_3 = 1.5 Å. The three-body term is always non-negative and prevents the formation of hydrogen clusters H_n for n > 2. For the study of the hydrogen dissociation reaction, all hydrogen atoms are initially bound in H_2 molecules, and the final state is reached when at least one bond is broken. A simple two-body repulsive potential can then be used to mimic the repulsive contribution from the three-body term, and, in the approximate model, the interaction consists of an intramolecular part (which is identical to the two-body term given in eq 11) and an intermolecular part, $V_{ij}^{inter}(\mathbf{r}_i, \mathbf{r}_j)$, which is evaluated between atoms in different molecules and modeled as a repulsive potential

$$V_{ij}^{inter}(r_{ij}) = \xi_2[\exp(\gamma_4(r_c - r_{ij})) - 1] \tag{15}$$

if $r_{ij} < r_c$, and zero otherwise. We have obtained parameters (γ_4 = 8.3826 Å and ξ_2 = 0.26239 kcal/mol) for this potential by fitting the forces obtained in the approximate description to the corresponding forces from the more detailed potential as described in the Appendix.

3. TEST CASES

We have considered several test cases for the two models presented in the previous section. In this section we briefly describe these cases, and we present results from RETIS simulations we carried out in order to select them. We postpone the description of the computational details to the next section where we present the results from using the new method on the test cases presented here.

As previously described, the strength of the solvent effect in the ion transfer potential can be tuned by changing f_c and R_{coop}. A larger f_c gives a stronger effect by increasing the contribution from the cooperative potential (see eqs 6 and 9), and a larger R_{coop} increases the coordination number which leads to a reduction in $H(n; N_c, N_n)$ and gives a stronger effect as well. We carried out RETIS simulations (without gluing) for a combination of parameters (R_{coop} and f_c), and the obtained rate constants are given (together with the parameters) in Table 2. These results show that the rate constant obtained by not including the cooperative effect can be several orders of magnitude lower than the rate constants obtained when the

DOI: 10.1021/acs.jctc.5b00012
J. Chem. Theory Comput. 2015, 11, 2440−2450

Table 2. Rate Constant for the Ion Transfer Reaction[a]

case	R_{coop}	f_c	k_{AB}
0 (without cooperativity)			(1.00 ± 0.06)
1	1.1	1/3	$(1.92 \pm 0.07) \times 10^1$
2	1.3	1/3	$(4.89 \pm 0.16) \times 10^2$
3	1.3	2/3	$(9.47 \pm 0.16) \times 10^5$
4	1.3	19/20	$(3.40 \pm 0.04) \times 10^9$

[a]All the rate constants are calculated relative to the rate constant for the case where the cooperative effect is ignored, $k_{AB} = (2.6 \pm 0.16) \times 10^{-11}$.

cooperative effect is included. Based on these RETIS simulations, cases 1−3 were selected for further investigation. The last case, 4, was not included as the rate constant here is relatively high.

For each of these cases we consider the following five variations which we label a)−e): a) "No gluing", corresponding to the usual RETIS approach; b) "Gluing", corresponding to the new QuanTIS method; c) RETIS with a swap frequency set to zero (which approximately corresponds to the TIS method); d) "Fewer interfaces" which corresponds to method b) with a reduced number of interfaces; and finally e) "Accept all", corresponding to artificially ignoring the detailed balance condition in eq 4 and accepting all swapping moves $[0^-] \leftrightarrow [0^+]$. In case d), the first interface was removed which implies that the new first interface λ_0 is shifted more into the barrier region so that the average path length of the low-level $[0^-]$ system becomes even longer with respect to the high-level description $[0^+]$ trajectories. These variations will allow us to discuss the new method and compare it with the RETIS and TIS approaches.

For the hydrogen potential, we carried out RETIS simulations for the dissociation at temperatures 1500, 2000, and 2500 K and a density of 0.07 g/cm^3. For these conditions, the stable phase of hydrogen is a molecular liquid and the dissociation is low.[37] At 1500 K, we estimate the thermal de Broglie wavelength to be approximately 0.45 Å which is comparable to the hydrogen bond length (0.74 Å) used in the model. To assess the impact of possible quantum mechanical effects, we have compared the radial distribution function for hydrogen at 600, 1000, and 1500 K using both the classical model and path integral simulations (see Figure 7 and the description in the Appendix), and we find that we can neglect such effect for the temperatures we consider. The rate constants we obtain by RETIS simulations are given in Table 3. For an efficiency analysis it is required to have well converged results for all methods, including the less efficient ones. We therefore focus on the 2000 and 2500 K cases which are more accessible than the 1500 K case. For this potential, we also consider the same variations a)−e) as for the ion exchange potential, and, in addition, we consider a sixth case: f) No gluing and using the approximate potential everywhere.

Table 3. Rate Constant for the Hydrogen Dissociation Reaction[a]

case	temp/K	k_{AB}
0	1500	$(2.91 \pm 0.15) \times 10^{-4}$
1	2000	(1.00 ± 0.03)
2	2500	$(1.84 \pm 0.04) \times 10^2$

[a]All rate constants are relative to the rate constant at 2000 K, $k_{AB} = (2.96 \pm 0.09) \times 10^{-6}$ ns^{-1}. Simulation details are given in the next section.

4. COMPUTATIONAL DETAILS

The equations of motion were propagated in time under NVE dynamics using the Velocity Verlet integrator[38] with periodic boundaries (in two dimensions for the ion potential and three dimensions for the hydrogen potential). In the RETIS simulations, 1×10^6 cycles were performed and the swapping probability was set to 50%, while the probabilities of performing time reversal moves or shooting moves were both set to 25%. We applied the simplified version[20] of aimless shooting[39] which implies that the velocities at the shooting point were generated from a Maxwellian distribution at the given temperature (0.1 in reduced units for the ion transfer; 2000 or 2500 K for the hydrogen dissociation), and the shooting points were picked with an equal probability along the path. The positions of the interfaces used in the RETIS calculation were placed to increase the efficiency of the method.[20,21]

For the ion potential, the time step was $\delta t = 0.002$ in reduced units, and the particles were assumed to have identical masses (of 1). Initially the ion, x, is bound to one of the A particles (labeled A_1), and it is transferred to the other A particle (labeled A_2) over the course of the reaction. The order parameter, λ, is defined using the distance between x and A_2 (r_{xA_2}), as

$$\lambda = -r_{xA_2} \tag{16}$$

where the minus sign is included just for convenience: The order parameters changes from a low value to a high value over the course of the ion transfer. The two stable states were defined as corresponding to $\lambda < -0.7$ and $\lambda > 0.4$, respectively, and interfaces were placed at positions −0.7, −0.64, −0.62, −0.60, −0.59, −0.58, −0.57, −0.56, −0.55, −0.54, −0.53, −0.52, −0.51, −0.50, and −0.45. Initially, the A and B particles were positioned on a regular 2D grid such that each particle was surrounded by 4 neighbors, all at a distance of 1.2 from each other. The unit cell was quadratic with a side length of 3.873 reduced units.

For the hydrogen potential, we define reduced units by the mass of the hydrogen atom, a length equal to 1 Å, and the binding energy of hydrogen (103.266 kcal/mol). The time unit is then τ = 4.81 fs, and the NVE simulations were performed with a time step of 0.1 τ. We considered 4 H_2 molecules in a cubic box with an edge length equal to 5.786 Å (corresponding to a density of 0.07 g/cm^3). Initially, we placed the molecules (i.e., their center of mass) on sites corresponding to a face-centered cubic lattice and oriented the molecules randomly. The initial velocities of the molecules were drawn from a Maxwellian distribution corresponding to the target temperature for the simulation (2000 or 2500 K).

The order parameter for the hydrogen reaction was obtained in the following way: For each pair of hydrogen atoms that were initially bound together in a H_2 molecule, we calculated the distance between the atoms. We then defined the order parameter as the maximum of these bond lengths. This unconventional reaction coordinate is one of the advantages of the TIS-based algorithms: It is much more flexible than for instance thermodynamic integration with respect to the range of reaction coordinates that can be chosen. Taking the maximum value of all intramolecular distances allows for dissociation of any H_2 molecule in the system which ensures a faster decorrelation than for the case that a single target molecule has to be selected beforehand. Since the method now calculates the rate constant that any H_2 molecules dissociates, the calculated rate constants for the hydrogen potential have been normalized with the number of hydrogen molecules to obtain the dissociation rate

DOI: 10.1021/acs.jctc.5b00012
J. Chem. Theory Comput. 2015, 11, 2440−2450

Table 4. Initial Flux (f_A), Crossing Probability ($\mathcal{P}_A(\lambda_B|\lambda_A)$), Rate Constant ($k_{AB}$), and Ratio of Path Lengths ($\langle t_{path}^{[0^-]}\rangle/\langle t_{path}^{[0^+]}\rangle$) for the Three Cases of the Ion Transfer Reaction: Case 1 with $R_{coop} = 1.1$ and $f_c = 1/3$; Case 2 with $R_{coop} = 1.3$ and $f_c = 1/3$; and Case 3 with $R_{coop} = 1.3$ and $f_c = 2/3$[a]

case 1	f_A	$\mathcal{P}_A(\lambda_B\|\lambda_A) \times 10^9$	$k_{AB} \times 10^{10}$	$\langle t_{path}^{[0^-]}\rangle/\langle t_{path}^{[0^+]}\rangle$	acceptance (%)
a)	0.476 ± 0.003	***1.05 ± 0.04***	5.0 ± 0.2	7.46 ± 0.05	
b)	***0.497 ± 0.003***	***1.17 ± 0.04***	***5.8 ± 0.2***	***7.09 ± 0.05***	97.6
c)	***0.495 ± 0.004***	***1.15 ± 0.06***	***5.7 ± 0.3***	***7.18 ± 0.07***	
d)	0.165 ± 0.001	3.4 ± 0.2	***5.6 ± 0.3***	84.2 ± 0.4	88.2
case 2	f_A	$\mathcal{P}_A(\lambda_B\|\lambda_A) \times 10^8$	$k_{AB} \times 10^8$	$\langle t_{path}^{[0^-]}\rangle/\langle t_{path}^{[0^+]}\rangle$	acceptance (%)
a)	0.371 ± 0.002	***3.41 ± 0.11***	1.26 ± 0.04	9.46 ± 0.06	
b)	***0.506 ± 0.004***	***3.33 ± 0.11***	***1.68 ± 0.06***	***6.67 ± 0.05***	82.6
c)	***0.501 ± 0.011***	***3.3 ± 0.2***	***1.69 ± 0.13***	***6.73 ± 0.16***	
d)	0.0946 ± 0.0004	13.9 ± 0.4	***1.31 ± 0.03***	132.6 ± 0.6	87.6
e)	0.483 ± 0.003	4.35 ± 0.14	2.10 ± 0.07	6.91 ± 0.05	100
case 3	f_A	$\mathcal{P}_A(\lambda_B\|\lambda_A) \times 10^4$	$k_{AB} \times 10^5$	$\langle t_{path}^{[0^-]}\rangle/\langle t_{path}^{[0^+]}\rangle$	acceptance (%)
a)	0.352 ± 0.002	***0.700 ± 0.011***	2.46 ± 0.04	9.45 ± 0.06	
b)	***0.553 ± 0.004***	***0.725 ± 0.012***	***4.01 ± 0.07***	***5.66 ± 0.05***	67.7
c)	***0.555 ± 0.005***	***0.725 ± 0.019***	***4.02 ± 0.11***	***5.64 ± 0.06***	
d)	0.165 ± 0.001	2.48 ± 0.03	***4.11 ± 0.06***	59.9 ± 0.2	66.1
e)	0.516 ± 0.003	1.041 ± 0.017	5.37 ± 0.09	5.85 ± 0.04	100

[a]The different variations of the simulation methods are a) the usual RETIS approach; b) the new QuanTIS method; c) RETIS with a swap frequency set to zero; d) QuanTIS with the first interface removed; e) RETIS where all swapping moves are artificially accepted (the detailed balance condition in eq 4 is ignored). Since the acceptance is relatively high in case 1b), we did not perform the "accept all" simulations case 1e) here. In each column, we have italicized the different quantities that should be identical within statistical uncertainties. All quantities are given in reduced units based on the ion transfer potential.

Table 5. Initial Flux f_A, Crossing Probability $\mathcal{P}_A(\lambda_B|\lambda_A)$, Rate Constant k_{AB}, and Ratio of Path Lengths $\langle t_{path}^{[0^-]}\rangle/\langle t_{path}^{[0^+]}\rangle$ for the Hydrogen Dissociation at 2000 and 2500 K[a]

2000 K	$f_A \times 10^{-4}/\text{ns}^{-1}$	$\mathcal{P}_A(\lambda_B\|\lambda_A) \times 10^{10}$	$k_{AB} \times 10^6/\text{ns}^{-1}$	$\langle t_{path}^{[0^-]}\rangle/\langle t_{path}^{[0^+]}\rangle$	acceptance (%)
a)	1.082 ± 0.008	***2.74 ± 0.08***	2.96 ± 0.09	9.45 ± 0.07	
b)	***1.086 ± 0.009***	***2.70 ± 0.08***	***2.93 ± 0.09***	***9.42 ± 0.09***	83.2
c)	***1.120 ± 0.010***	***2.50 ± 0.06***	***2.79 ± 0.07***	***9.15 ± 0.09***	
d)	0.183 ± 0.003	20 ± 1	***3.65 ± 0.13***	70 ± 1	82.9
e)	1.064 ± 0.010	2.76 ± 0.09	2.94 ± 0.11	9.58 ± 0.10	100
f)	1.090 ± 0.011	1.97 ± 0.07	2.14 ± 0.08	9.41 ± 0.10	
2500 K	$f_A \times 10^{-4}/\text{ns}^{-1}$	$\mathcal{P}_A(\lambda_B\|\lambda_A) \times 10^8$	$k_{AB} \times 10^4/\text{ns}^{-1}$	$\langle t_{path}^{[0^-]}\rangle/\langle t_{path}^{[0^+]}\rangle$	acceptance (%)
a)	1.667 ± 0.010	***3.26 ± 0.07***	5.44 ± 0.13	4.82 ± 0.03	
b)	***1.670 ± 0.011***	***3.03 ± 0.07***	***5.06 ± 0.12***	***4.81 ± 0.04***	85.6
c)	***1.684 ± 0.013***	***3.03 ± 0.06***	***5.09 ± 0.11***	***4.78 ± 0.04***	
d)	0.415 ± 0.004	14.0 ± 0.3	***5.8 ± 0.2***	26.6 ± 0.3	85.3
e)	1.655 ± 0.011	3.29 ± 0.08	5.45 ± 0.13	4.82 ± 0.04	100
f)	1.680 ± 0.012	2.24 ± 0.06	3.7 ± 0.10	4.80 ± 0.04	

[a]The different variations of the simulation methods a)−e) are the same as defined in Table 4, while the additional case f) corresponds to RETIS where the approximate potential is used everywhere. In each column, we have italicized the different quantities that should be identical within statistical uncertainties.

constant for a single molecule. The initial and final states for the hydrogen reaction corresponds to $\lambda < 0.9$ Å and $\lambda > 2.4$ Å, respectively. We considered interfaces placed at positions (in units of Å): 0.95, 1.05, 1.15, 1.25, 1.30, 1.35, 1.40, 1.50, 1.60, 1.75, 1.90, 2.10, 2.20, 2.30, and 2.40.

5. RESULTS AND DISCUSSION

We have calculated the initial flux (f_A), the overall crossing probability ($\mathcal{P}_A(\lambda_B|\lambda_A)$), the rate constant ($k_{AB}$), and the ratio of the average path lengths in the $[0^-]$ and $[0^+]$ ensembles ($\langle t_{path}^{[0^-]}\rangle/\langle t_{path}^{[}0^+]\rangle$) for the different cases we considered for the two potentials. The results for the ion transfer are presented in Table 4 and for the hydrogen dissociation in Table 5. The individual crossing probabilities are shown for case 3 of the ion potential in Figure 1 and for the hydrogen dissociation at 2500 K in Figure 2.

Overall we find good agreement for the obtained rate constants when we compare the results for the RETIS method with and without gluing. The results from the RETIS simulations where the swapping frequency is set to zero are in close agreement with the simulations where the swapping frequency is 50%, as expected.

We do find variations up to about 50% in the rate constant for the ion potential when we compare RETIS with QuanTIS, see for instance case 2a) and b) and case 3a) and b) in Table 4. This is caused by an increased initial flux when we apply the approximate potential in the $[0^-]$ ensemble. The conditional crossing probabilities (see Figure 1) remain unchanged within the uncertainty, as long as the positions of the interfaces are unchanged, and as long as the detailed balance condition is respected. Ignoring the detailed balance condition, eq 4, and

DOI: 10.1021/acs.jctc.5b00012
J. Chem. Theory Comput. 2015, 11, 2440−2450

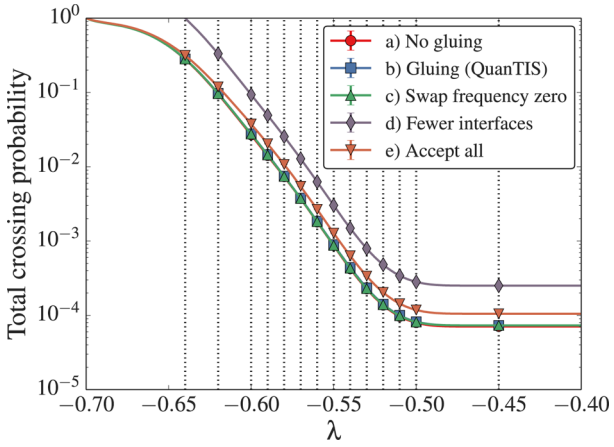

Figure 1. Crossing probabilities as a function of the order parameter for case 3 of the ion potential (R_{coop} = 1.3 and f_c = 2/3). The positions of the interfaces are indicated with vertical dotted lines. The different cases included here are a) the RETIS approach without gluing (circles, color red); b) the QuanTIS method (squares, color blue); c) RETIS with a swap frequency set to zero (triangles, color green); d) QuanTIS with the first interface removed (diamonds, color purple); e) RETIS where all swapping moves are artificially accepted (down-pointing triangle, color orange).

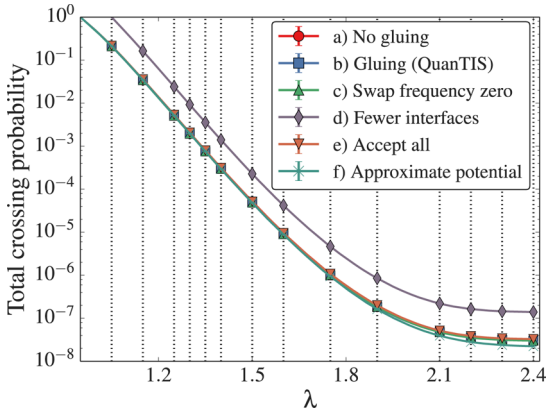

Figure 2. Crossing probabilities as a function of the order parameter for the hydrogen dissociation at 2500 K. The positions of the interfaces are indicated with vertical dotted lines. The different cases included here are a) the RETIS approach without gluing (circles, color red); b) the new QuanTIS method (squares, color blue); c) RETIS with a swap frequency set to zero (triangles, color green); d) QuanTIS with the first interface removed (diamonds, color purple); e) RETIS where all swapping moves are artificially accepted (down-pointing triangle, color orange); f) RETIS where the approximate potential is used everywhere (crosses, color cyan).

accepting all swapping moves $[0^-]\leftrightarrow[0^+]$ leads to an overestimation of the crossing probability (and rate constant): see cases 2e) and 3e) in Table 4. Inspection of Figure 1 shows, however, that for $i \geq 3$ all conditional crossing probabilities $\mathcal{P}_A(\lambda_{i+1}|\lambda_i)$ of the accept-all approach give the correct values as follows from the total crossing probability which is essentially running parallel to the other results in the logarithmic plot after $\lambda_3 = -0.6$.

We note that although the initial flux and the overall crossing probability seems to differ significantly when we change the positions of the interfaces, the rate constants should still be identical. This is due to the fact that a rate constant is obtained as the product of the initial flux and the overall crossing probability. This can for instance be seen in Table 4 for case 3b) and 3d) where the smaller initial flux in case 3d) gives a proportionally larger crossing probability and the rate constant remains approximately constant. Case 3d) also show that we can modify the ratio of the path lengths by placing the interfaces differently. Here, it is simply done by removing the first interface. This is beneficial for two reasons: (1) the number of interfaces is decreased, and (2) the path lengths in the $[0^-]$ ensemble are increased, which in turn will increase the gain of using the QuanTIS method.

For the hydrogen dissociation, we do not see a large effect on the initial flux when using the approximate potential, compare cases a) and b) in Table 5. All the path lengths in the first two ensembles are relatively short in cases a) and b) (on average approximately 50 steps) for the conditions we have considered, and there is not much room for variation. By removing the first interface, we obtain longer path lengths, and we see a decrease in the initial flux and a corresponding increase in the crossing probability.

However, in this case we see a larger discrepancy when comparing the d) cases with cases b) and c): The rate constant for the d) cases appear to be overestimated. In the current implementation of the method, we store all timeslices of the paths, and we restrict the length of these paths to a fixed value (20000 timeslices). When we remove the first interface, the path lengths become larger on average and may more often exceed the preset maximum length. This will effectively lead to an overestimation of the initial flux f_A and subsequently of k_{AB}, since very long paths in the $[0^-]$ ensemble may artificially be rejected. For case d) at 2000 K, the maximum allowed path lengths were increased to 80000 timeslices in order to increase the accuracy. We are currently developing a method to circumvent this potential problem.

To further investigate the efficiency of the new method, we have also calculated the efficiency times, $\tau_{\text{eff}}^{[i^+]}$, given by[21]

$$\tau_{\text{eff}}^{[i^+]} = \frac{1 - p_i}{p_i} \xi_i L_i N_i \tag{17}$$

where $p_i = \mathcal{P}_A(\lambda_{i+1}|\lambda_i)$, $L_i = \langle t_{\text{path}}^{[i^+]} \rangle / \delta t$, N_i is the effective correlation between trajectories, and ξ_i is the ratio between the average cost of the simulation cycle and L_i. The efficiency times can be interpreted as the minimum computational cost (e.g., force calculations needed) to obtain an overall relative error equal to 1.[40] For the ion potential, setting the swap frequency to zero has a dramatic effect on the efficiency times, see Figure 3. The overall efficiency time for case 3c) is approximately 135360/276005 ≈ 5 times the overall efficiency time for case 3b). This is caused by a much faster decorrelation (as measured by N_i) for the case when the swapping moves are used. It is also reflected in ξ_i which is consistently larger for case 3c). The improved efficiency of QuanTIS compared to RETIS is not reflected in these data since efficiency times are expressed in the number of force evaluations. Hence, this analysis does not take into account that the force evaluations in the lower level description can in practice be a few thousand times faster than in the higher level description, as in the combination of classical MD with DFT-based MD.

For the hydrogen potential, the effect of setting the swapping frequency to zero is not so pronounced. In this case ξ_i is larger for the case with a zero swapping frequency; however, the effective correlation between the trajectories is relatively low, and the all

DOI: 10.1021/acs.jctc.5b00012
J. Chem. Theory Comput. 2015, 11, 2440−2450

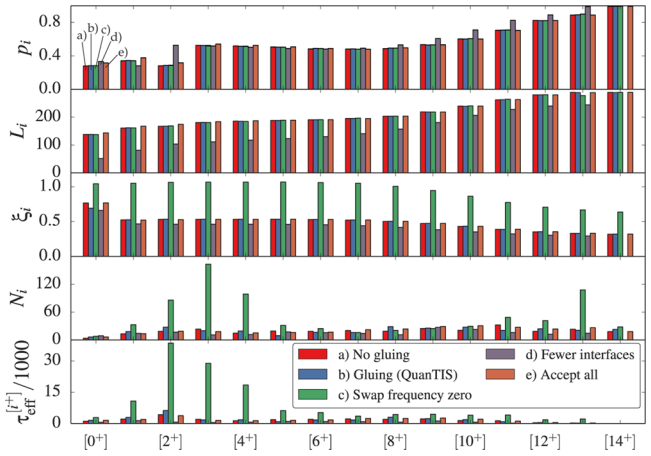

Figure 3. Calculated efficiencies for the RETIS/QuanTIS simulations for case 3 of the ion transfer potential (R_{coop} = 1.3 and f_c = 2/3). From top to bottom: The conditional crossing probability $p_i = \mathcal{P}_A(\lambda_{i+1}|\lambda_i)$, with the average path length being L_i, the ratio between the average cost of the simulation cycle and the average path length being ξ_i, the effective correlation between trajectories being N_i, and the efficiency times being $\tau_{eff}^{[i^+]}$. The efficiency times were calculated as described in the text. The different cases included here are a) the RETIS approach without gluing (color red); b) the new QuanTIS method (color blue); c) RETIS with a swap frequency set to zero (color green); d) QuanTIS with the first interface removed (color purple); e) RETIS where all swapping moves are artificially accepted (color orange).

path lengths are short, giving a smaller effect. In fact, the ratio of the efficiency times is approximately 6780/5496 ≈ 1.23 when comparing the case with swap frequency zero to the case with a swap frequency equal to 50%. This difference is mainly caused by the larger ξ_i in the former case.

6. PROSPECTS

Since the energy is an extensive quantity we can expect that the acceptance in eq 4 will drop for large systems. There are several possibilities to circumvent this problem. One possibility is to mix the two potentials using e.g. an alternative potential V'_{lo} at the lower level

$$V'_{lo}(\lambda) = H(\lambda, \Lambda_c, \Lambda_n)V_{lo} + ((1 - H(\lambda, \Lambda_c, \Lambda_n))V_{hi} \quad (18)$$

where H is the smooth step function that goes from 1 to 0 as previously defined in eq 8, and Λ_c and Λ_n are parameters determining the position and the steepness of this inflection, respectively. Λ_c should be placed somewhere around the first interface. For λ values far lower than Λ_c the potential is simply V_{lo} and expensive quantum calculations are not needed, but each time that λ approaches the first interface some force field evaluations at the V_{hi} will be required. However, once the exchange move is attempted, the acceptance probability should be much higher. The gradual increase of the high level description could in principle also be extended to the other path ensembles, or the QuanTIS method could be combined with standard QM-MM which reduces the region in which there is a mismatch.

An exciting idea that we plan to investigate is to adapt parameters of a classical potential during the simulation in a similar fashion as force-matching[41] or learning-on-the-fly.[42] Since the acceptance probability of eq 4 is maximized when V_{lo} and V_{hi} are similar at the first interface, the average acceptance probability provides a natural cost function that can be optimized. This approach has two benefits: first of all it will enhance the efficiency of the QuanTIS method, and, second, it will provide an accurate force field which could be used in a multiscale scheme. The algorithm that we plan to test is to update a database of configurations $\{r_{lo}, r_{hi}\}$ each time that the replica exchange move is attempted. Then, after a certain number of replica exchange moves, the force field parameters are adjusted in order to maximize following cost function

$$Q \equiv \frac{\sum_{j,k} w^j P_{acc}(r_{lo}^j, r_{hi}^k)}{N_{swaps} \sum_j w^j} \quad (19)$$

where N_{swaps} are the number of replica exchange moves performed so far, and j, k are indexes of the different configuration points generated via V_{lo} and V_{hi}, respectively. w_j are weights corresponding to the $\{r_{lo}\}$ points which we will discuss later on. As P_{acc} depends on V_{lo}, Q depends on force field parameters which determine this potential, and optimization routines in parameter space can be applied to maximize Q. The optimization of this cost function has specific advantages compared to standard parameter fitting schemes. One advantage already mentioned is that it is directly linked to the efficiency of the QuanTIS method. Another advantage is that it is well-defined; there is no need to tune predefined required accuracies of dissimilar properties like bond distances, energies, angles, etc. Moreover, the configurations that are sampled are relevant for the reaction under study. Manually created benchmark data using quantum calculations often focus too strongly on minimum energy configurations and transition states which might not be relevant for the temperature that is considered in the actual simulation. Finally, the Q function tests the accuracy of the V_{lo} force field from both perspectives; not only should the force field mimic the energies of the geometries from the quantum data, the points generated by V_{lo} are also analyzed. Reactive force fields, fitted on high level quantum mechanical data, can simulate spurious reactions which naturally were never considered during the design of the Ab Initio database. In this scheme such unphysical behavior would directly be penalized. However, suppose the classical force field generates a point r_{lo}^j with a corresponding unrealistically high energy $V_{hi}(r_{lo}^j)$. In that case, it would be sufficient to change the parameters of V_{lo} such that this point will never be generated again. Requiring that $V_{lo}(r_{lo}^j) \approx V_{hi}(r_{lo}^j)$ would put a too strong restriction on the parameter set since this point r_{lo}^j has become irrelevant in the next update of the V_{lo} potential. It is therefore that we put a weight w^j in the expression which should be proportional to the relevance of the r_{lo} points. There are several practical solutions how to define appropriate weights, but it is yet far from trivial to predict what is the most effective way to do so. One natural requirement is that the weights should not change, at least not relatively, when adding a trivial constant to the potential V_{lo}. We shall report on these technicalities in forth-coming publications.

7. CONCLUSION

We have introduced the new method QuanTIS that glues different potential energy surfaces in order to model rare transitions such as chemical reactions. In this way, QuanTIS allows using different levels of theory to describe distinct subprocesses of this transition. One interesting application is to use QuanTIS to study chemical reactions in a solvent in which the breaking and making of chemical bonds is done by accurate Ab Initio MD, while the diffusion of reactants is treated by

DOI: 10.1021/acs.jctc.5b00012
J. Chem. Theory Comput. 2015, 11, 2440−2450

classical force fields. The new method is based on the previously developed RETIS[20] method which already gives a dramatic increase in efficiency compared to brute-force MD. By adjusting the acceptance rule of the replica exchange move between the different path simulations, we can maintain detailed balance and increase the efficiency even further in the QuanTIS method.

Both in the RETIS and in the QuanTIS scheme the rate constant of the transition is calculated from a flux factor f_A times the overall crossing probability $\mathcal{P}_A(\lambda_B|\lambda_A)$. In the QuanTIS scheme the flux factor will be mainly determined by the potential energy surface V_{lo} that is based on the lower level theory. The crossing probability will be purely determined on the higher level potential V_{hi}. Hence, $\mathcal{P}_A(\lambda_B|\lambda_A)$ is not affected by V_{lo}, but the efficiency of its computation certainly will. The replica exchange moves between the two systems reduce significantly the correlation between trajectories in all path ensembles. By positioning the first interface far into the barrier region, the path on the cheap V_{lo} potential can be made very long, and an exchange move to the V_{hi} potential, if accepted, is likely to generate a path that is completely uncorrelated to the previous path in that ensemble.

In this article we give the first proof-of-concept of this new approach by applying it on two model systems. The first system describes a hypothetical ion transport model in which we exclude or include cooperative effects in the V_{lo} and V_{hi} potentials, respectively. In a second stage, we also applied it to the dissociation of hydrogen based on a reactive force field from the literature.[35] In this model we ignored the three-body term of the hydrogen potential in the lower description but added a simple repulsive steep potential to obstruct trimer formations. Our results show that the crossing probability $\mathcal{P}_A(\lambda_B|\lambda_A)$ is indeed converging to the same results as in the RETIS simulations using the high-level description on all path ensembles.

We note that the acceptance of the swapping between the two levels of theory can drop for large systems, and we have discussed possible solutions to this problem (see e.g. eq 18). For the systems that we studied this was not the case. The realistic hydrogen model even showed acceptance close to 100% after a simple optimizing procedure for positioning the repulsive potential. The results for the detailed-balance violating "accept-all" approach shows that only the very first crossing probabilities are affected. This suggests that the "accept-all" approach might be a practical method if an approximate value for the reaction rate (within 1 order of magnitude) is sufficient.

In conclusion, we believe that the QuanTIS method is a promising method to connect different levels of theory for studying rare transitions. In addition, it also provides interesting prospectives regarding force field optimization which are presently under investigation.

A. APPENDIX

A.1. Detailed Description of the Interaction Potentials. In the ion potential, the pair interaction is based on the Lennard-Jones potential, V_{LJ}^{ij}

$$V_{LJ}^{ij}(r_{ij}) = 4\epsilon_{ij}\left[\left(\frac{\sigma_{ij}}{r_{ij}}\right)^{12} - \left(\frac{\sigma_{ij}}{r_{ij}}\right)^{6}\right] \tag{20}$$

where ϵ_{ij} and σ_{ij} are the parameters for the potential. The form of the pair interaction between particles of type A and x is given by a shifted Lennard-Jones potential

$$V_{Ax}(r_{Ax}) = V_{xA}(r_{xA}) = \begin{cases} V_{LJ}^{xA}(r_{xA}) - V_{LJ}^{xA}(r_{xA}^c), & \text{if } r_{xA} < r_{xA}^c \\ 0, & \text{if } r_{xA} \geq r_{xA}^c \end{cases} \tag{21}$$

and the other interactions are modeled by the Weeks–Chandler–Andersen (WCA) potential

$$V_{ij}^{WCA}(r_{ij}) = \begin{cases} V_{LJ}^{ij}(r_{ij}) + \epsilon_{ij}, & \text{if } r_{ij} < r_{ij}^c \\ 0, & \text{if } r_{ij} \geq r_{ij}^c \end{cases} \tag{22}$$

with cut-offs given by $r_{ij}^c = 2^{1/6}\sigma_{ij}$. The cluster energy is given by the interactions between the two A particles labeled A_1 and A_2 and the x particle

$$V_{cluster} = V_{xA_1}(r_{xA_1}) + V_{xA_2}(r_{xA_2}) + V_{A_1A_2}^{WCA}(r_{A_1A_2}) \tag{23}$$

Here, V_{xA_1} and V_{xA_2} are modeled with the shifted Lennard-Jones potential, while $V_{A_1A_2}$ is given by the WCA potential. In Figure 4 we illustrate the effect of cooperation on the interaction.

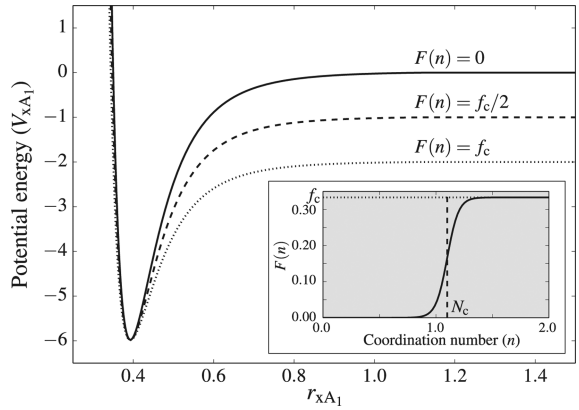

Figure 4. Illustration of the cooperative effect on the x–A interaction. The figure shows the potential energy as a function of the distance (both in reduced units) between the x particle and one A particle (labeled A_1) in the presence of B particles. The second A particle is assumed to be at a distance where the interaction with x can be neglected. The solid line corresponds to the case where the coordination number is zero, the dashed line to a case where the coordination number is intermediate (here: equal to N_c), and the dotted line corresponds to the case where the coordination number is high. The inset shows the variation of $F(n)$ with respect to the coordination number for $N_c = 1.1$, $N_n = 20$, and $f_c = 1/3$.

In Figure 5 we illustrate the hydrogen potential and elaborate the triplet notation we have used in the main text.

A.2. Parameters for the Approximate Hydrogen Potential. The two parameters for the approximate hydrogen potential were obtained by fitting the simplified potential to the more detailed potential in the following way: First, the more detailed potential was used to run a short simulation (10^6 steps with a time step of 0.1 in reduced units) of 32 particles in a cubic box (box length 9.1843 Å) with NVT dynamics and a temperature corresponding to 1500, 2000, and 2500 K. The positions ($\mathbf{r}_i$) and forces ($\mathbf{f}_i$) on all the atoms in the system were stored every 10th step. We then re-evaluated the forces using the approximate potential and used the Levenberg–Marquardt algorithm[43,44] to optimize the parameters γ_4 and ξ_2. This was done by minimizing the function g defined as

DOI: 10.1021/acs.jctc.5b00012
J. Chem. Theory Comput. 2015, 11, 2440–2450

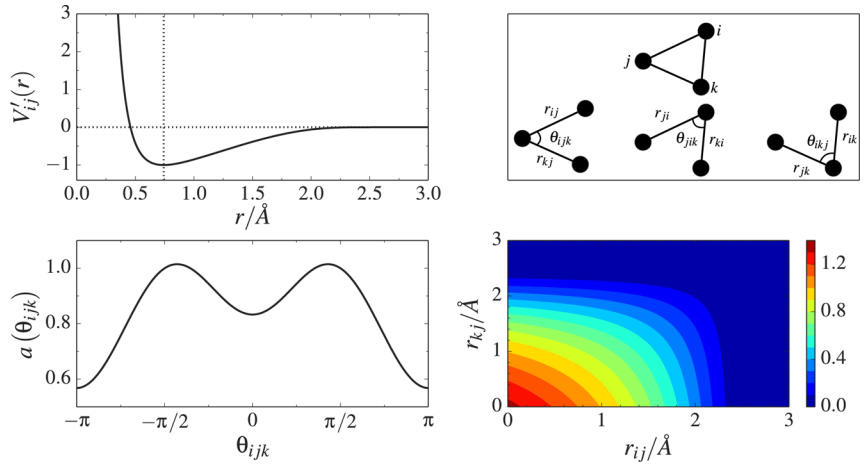

Figure 5. Illustration of the two- and three-body potential energy. (Top-left) The pair interaction scaled ($V'_{ij}(r)$) with the bond energy of hydrogen, 103.266 kcal/mol.[35] The minimum of the pair interaction occurs at a distance of $r \approx 0.74$ Å (vertical dotted line) which corresponds to the bond distance in H_2. (Top-right) The notation for the triplet interactions and angles. (Bottom-left) The angle term of the three-body interaction. (Bottom-right) The angle-independent part of the three-body term (i.e., $\lambda \exp[\gamma_3/(r_{ij}-r_c) + \gamma_3/(r_{kj}-r_c)] \geq 0$).

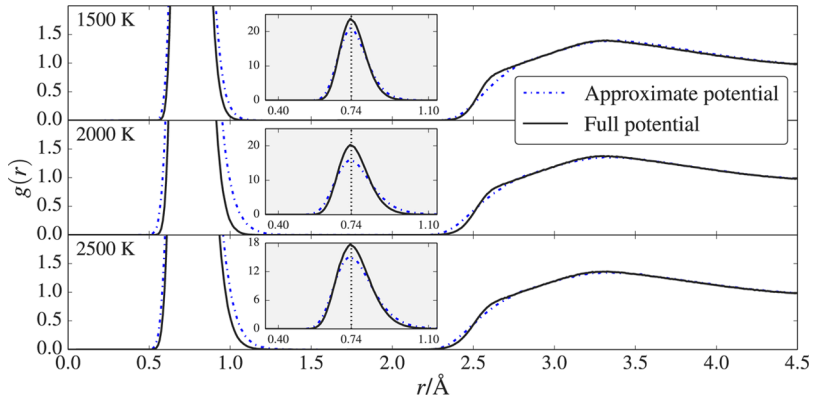

Figure 6. Radial distribution function $g(r)$ for the full (solid line) and approximate (dashed line) potential for temperatures (from top to bottom) 1500, 2000, and 2500 K. The insets are closeups of the peaks around 0.74 Å.

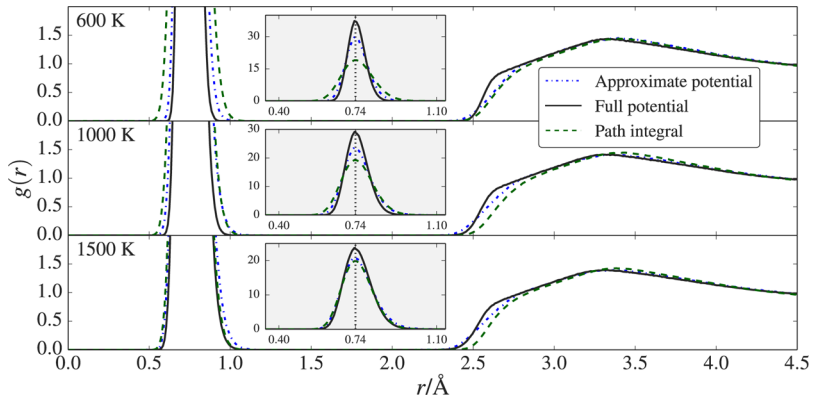

Figure 7. Radial distribution function $g(r)$ for the full (solid line) and approximate (dashed line) potential for temperatures (from top to bottom) 600, 1000, and 1500 K. The insets are close-ups of the peaks around 0.74 Å.

$$g = \left(\sum_{k} \sum_{i=1}^{N} (\mathbf{f}_i - \mathbf{f}'_i)^2 \right)^{1/2} \tag{24}$$

where the first sum is over the recorded time steps, the second sum is over the N particles, and $\mathbf{f}'_i = \mathbf{f}'_i(\mathbf{r}_i(t_k); \gamma_4, \xi_2)$ represents the force on particle i evaluated using the approximate potential. As a simple comparison of the approximate and full potentials, we have evaluated the radial distribution functions at 1500, 2000, and 2500 K in Figure 6.

A.3. Path Integral Simulations of Molecular Hydrogen. In order to investigate the impact of possible quantum mechanical effects for the hydrogen potential, we have carried out path integral simulations of molecular hydrogen and obtained the one particle distribution function. We adopted the quantum-classical isomorphism introduced by Feynman and Hibbs[45] where the

DOI: 10.1021/acs.jctc.5b00012
J. Chem. Theory Comput. 2015, 11, 2440−2450

original quantum system is replaced by an auxiliary system in which each hydrogen atom is represented by a ring polymer made of P beads. We considered three temperatures, 600, 1000, and 1500 K, where P was set equal to 16, 8, and 4, respectively. These values of P are certainly below the values that ensure strict convergence of the quantum-classical correspondence, but by doubling P at 1000 K we verified that the simulations were converged to within a few percent. These simulations were carried out with 864 hydrogen atoms in a cubic box at a density of 0.07 g/cm^3, and we used a classical molecular dynamics method to sample the phase space.[46] The time step was 0.12 fs, and after equilibration (approximately 1.2 ns) statistics were accumulated over 1.8 ns.

The obtained distribution functions for the different temperatures are shown in Figure 7 and compared with the two classical models. The results show that the one particle density of each proton spreads over a Gaussian whose width is well described by the de Broglie thermal length. Comparison with the classical simulation shows that the intramolecular peak of the radial distribution function is significantly affected by quantum effects, since, with decreasing temperature, its height does not grow indefinitely as in the classical case but remains constant below 1000 K. More importantly, quantum effects on the intermolecular peaks are limited and of comparable size from 1500 K down to 600 K. Our conclusion, therefore, is that quantum effects are modest and could not change the results of the previous sections in any significant way; however, for temperatures below 600 K we expect that quantum effects may be important.

AUTHOR INFORMATION

Corresponding Author

*E-mail: titus.van.erp@ntnu.no.

Notes

The authors declare no competing financial interest.

ACKNOWLEDGMENTS

We are grateful to Prof. Pietro Ballone for kindly providing his programs and assistance for performing the path integral simulations using the hydrogen model to estimate the quantum nature of the hydrogen molecules. The authors thank the Research Council of Norway project no. 237423 and the Faculty of Natural Sciences and Technology (NTNU) for support.

REFERENCES

(1) Voter, A. F. *J. Chem. Phys.* **1997**, *106*, 4665−4677.
(2) Voter, A. F. *Phys. Rev. B* **1998**, *57*, R13985−R13988.
(3) Voter, A. F.; Sørensen, M. R. *Mater. Res. Soc. Symp. Proc.* **1999**, *538*, 427.
(4) Grubmüller, H. *Phys. Rev. E* **1995**, *52*, 2893−2906.
(5) Laio, A.; Parrinello, M. *Proc. Natl. Acad. Sci. U. S. A.* **2002**, *99*, 12562−12566.
(6) Carter, E.; Ciccotti, G.; Hynes, J. T.; Kapral, R. *Chem. Phys. Lett.* **1989**, *156*, 472−477.
(7) Torrie, G. M.; Valleau, J. P. *Chem. Phys. Lett.* **1974**, *28*, 578−581.
(8) Cerjan, C. J.; Miller, W. H. *J. Chem. Phys.* **1981**, *75*, 2800−2806.
(9) Barkema, G. T.; Mousseau, N. *Phys. Rev. Lett.* **1996**, *77*, 4358−4361.
(10) Henkelman, G.; Jónsson, H. *J. Chem. Phys.* **2000**, *113*, 9978−9985.
(11) Weinan, E.; Ren, W.; Vanden-Eijnden, E. *Phys. Rev. B* **2002**, *66*, 052301.
(12) Doye, J.; Wales, D. *Z. Phys. D: At., Mol. Clusters* **1997**, *40*, 194−197.
(13) Frenkel, D.; Smit, B. *Understanding molecular simulation*; Academic Press: San Diego, CA, 2002.
(14) Dellago, C.; Bolhuis, P. G.; Csajka, F. S.; Chandler, D. *J. Chem. Phys.* **1998**, *108*, 1964−1977.
(15) Bolhuis, P. G.; Dellago, C.; Chandler, D. *Faraday Discuss.* **1998**, *110*, 421−436.
(16) Dellago, C.; Bolhuis, P. G.; Chandler, D. *J. Chem. Phys.* **1999**, *110*, 6617−6625.
(17) Bolhuis, P. G.; Chandler, D.; Dellago, C.; Geissler, P. L. *Annu. Rev. Phys. Chem.* **2002**, *53*, 291−318.
(18) Dellago, C.; Bolhuis, P. G.; Geissler, P. L. In *Advances in Chemical Physics*; Prigogine, I., Rice, S. A., Eds.; John Wiley & Sons, Inc.: 2003; Vol. *123*; pp 1−78.
(19) van Erp, T. S.; Moroni, D.; Bolhuis, P. G. *J. Chem. Phys.* **2003**, *118*, 7762−7774.
(20) van Erp, T. S. *Phys. Rev. Lett.* **2007**, *98*, 268301.
(21) van Erp, T. S. *Comput. Phys. Commun.* **2008**, *179*, 34−40.
(22) Bolhuis, P. G. *J. Chem. Phys.* **2008**, *129*, 114108.
(23) Klenin, K. V.; Wenzel, W. *J. Chem. Phys.* **2010**, *132*, 104104.
(24) Borrero, E. E.; Dellago, C. *J. Chem. Phys.* **2010**, *133*, 134112.
(25) Gobbo, G.; Laio, A.; Maleki, A.; Baroni, S. *Phys. Rev. Lett.* **2012**, *109*, 150601.
(26) Juraszek, J.; Saladino, G.; van Erp, T. S.; Gervasio, F. L. *Phys. Rev. Lett.* **2013**, *110*, 108106.
(27) Warshel, A.; Levitt, M. *J. Mol. Biol.* **1976**, *103*, 227−249.
(28) Gao, J.; Xia, X. *Science* **1992**, *258*, 631−635.
(29) Quaytman, S. L.; Schwartz, S. D. *Proc. Natl. Acad. Sci. U. S. A.* **2007**, *104*, 12253−12258.
(30) Li, W.; Gräter, F. *J. Am. Chem. Soc.* **2010**, *132*, 16790−16795.
(31) Knott, B. C.; Haddad Momeni, M.; Crowley, M. F.; Mackenzie, L. F.; Götz, A. W.; Sandgren, M.; Withers, S. G.; Ståhlberg, J.; Beckham, G. T. *J. Am. Chem. Soc.* **2014**, *136*, 321−329.
(32) Gräter, F.; Li, W. In *Molecular Modeling of Proteins*; Kukol, A., Ed.; Methods in Molecular Biology; Springer: New York, 2015; Vol. *1215*; pp 27−45.
(33) Li, H., Yang, W. *J. Chem. Phys.* **2007***126*.
(34) Demontis, P.; Gulín-González, J.; Masia, M.; Suffritti, G. B. *J. Phys.: Condens. Matter* **2010**, *22*, 284106.
(35) Kohen, D.; Tully, J. C.; Stillinger, F. H. *Surf. Sci.* **1998**, *397*, 225−236.
(36) Skorpa, R.; Simon, J.-M.; Bedeaux, D.; Kjelstrup, S. *Phys. Chem. Chem. Phys.* **2014**, *16*, 1227−1237.
(37) Saumon, D.; Chabrier, G. *Phys. Rev. A* **1991**, *44*, 5122−5141.
(38) Verlet, L. *Phys. Rev.* **1967**, *159*, 98−103.
(39) Peters, B.; Trout, B. L. *J. Chem. Phys.* **2006**, *125*, 054108.
(40) van Erp, T. S. *J. Chem. Phys.* **2006**, *125*, 74106.
(41) Zhou, Y.; Pu, J. *J. Chem. Theory. Comput.* **2014**, *10*, 3038−3054.
(42) Csányi, G.; Albaret, T.; Payne, M.; De Vita, A. *Phys. Rev. Lett.* **2004**, *93*, 175503.
(43) Levenberg, K. *Q. Appl. Math.* **1944**, *2*, 164−168.
(44) Marquardt, D. W. *SIAM J. Appl. Math.* **1963**, *11*, 431−441.
(45) Feynman, R.; Hibbs, A. *Quantum mechanics and path integrals*; McGraw-Hill: 1965.
(46) Parrinello, M.; Rahman, A. *J. Chem. Phys.* **1984**, *80*, 860−867.

DOI: 10.1021/acs.jctc.5b00012
J. Chem. Theory Comput. 2015, 11, 2440−2450